Electrical detection of nuclear spins via silicon vacancies in silicon carbide at room temperature

View Online　Export Citation　CrossMark

Tetsuri Nishikawa,[1,2] Naoya Morioka,[1,3,a] Hiroshi Abe,[4] Hiroki Morishita,[1,3] Takeshi Ohshima,[4]
and Norikazu Mizuochi[1,3,a]

AFFILIATIONS

[1]Institute for Chemical Research, Kyoto University, Uji 611-0011, Japan
[2]Department of Molecular Engineering, Graduate School of Engineering, Kyoto University, Nishikyo-Ku 615-8510, Japan
[3]Center for Spintronics Research Network, Institute for Chemical Research, Kyoto University, Uji 611-0011, Japan
[4]National Institutes for Quantum Science and Technology, Takasaki 370-1292, Japan

[a]Authors to whom correspondence should be addressed: morioka.naoya.8j@kyoto-u.ac.jp and mizuochi@scl.kyoto-u.ac.jp

ABSTRACT

Color centers in wide-bandgap semiconductors, including diamond and silicon carbide (SiC), are attractive systems for quantum information and quantum sensor devices with excellent spin properties at room temperature. In addition, nuclear spins in crystals are expected to serve as the quantum memory and to enhance the sensitivity of quantum sensors with the combination with color centers as a result of an extremely long spin coherence time. Although the spin state of both color centers and nuclear spins coupled through hyperfine interactions is usually optically read out, an electrical readout technique is important for miniaturizing and integrating devices. In the present study, we report the electrical detection of silicon vacancy (V2) centers in 4H-SiC by photocurrent-detected magnetic resonance (PDMR) using a frequency-sweep technique. We electrically observe the spin coherence of the V2 centers and clearly resolve the hyperfine splitting of the electron spin signal for the V2 centers coupled with next-nearest-neighbor ^{29}Si atoms. In addition, we apply PDMR to electron–nuclear double resonance (PD-ENDOR) to detect nuclear magnetic resonance of ^{29}Si at room temperature and find that this method can resolve nuclear spins coupled with neighboring electron spins in the V2 centers. The realization of PD-ENDOR is expected to be a critical step toward the development of electrically driven integrated quantum devices.

Spin-active color centers in wide-bandgap semiconductors are attracting considerable attention for their potential applications in quantum information, quantum communication, and quantum sensor devices.[1–5] The nitrogen-vacancy (NV) center in diamond is the most studied system for quantum sensor[6–9] and quantum information processing applications.[10–13] In addition, color centers in silicon carbide (SiC), including divacancies,[14–16] silicon vacancies,[17–21] and nitrogen vacancies,[22–24] are also expected to function as quantum device platforms. In addition to the spin properties of its color centers, SiC's high device compatibility and material scalability are expected to contribute to the realization of scalable integrated quantum device technology.

In semiconductors, nuclear spins are another valuable quantum information resource. Nuclear spins exhibit excellent spin coherence properties at room temperature because they are less susceptible to surrounding environmental noise. Thus, they are considered promising candidates for quantum memory in information devices[25–27] and for enhancing sensitivity of quantum sensors.[28–30] Nuclear spins are

accessible via coupled electron spins of neighboring color centers through the hyperfine interaction. For instance, with the combination of an NV center and its ^{14}N or ^{15}N or neighboring ^{13}C nuclear spin, the readout of the nuclear spin state in diamond was demonstrated.[10,12,26,27,31,32]

One of the critical technologies for realizing integrated quantum devices is the electrical spin-state detection. Quantum information stored in color center spin is usually optically read out by spin-dependent fluorescence; however, direct electrical readout of spin information enables the miniaturization and simplification of devices. Previous research on NV centers in diamond[33–38] has demonstrated electrical readout of the spin state by photocurrent-detected magnetic resonance (PDMR) at room temperature, where a spin-dependent photocurrent is generated by laser excitation and detected with electrical contacts. PDMR of electron spins in V2 centers in 4H-SiC, which have a negatively charged Si vacancy at cubic sites,[39] was also demonstrated using an n^+/n^-/semi-insulating epitaxial structure.[40] The previous study avoided the influence of frequency-dependent

radiofrequency (RF) coupling noise by using the external-magnetic-field-sweep technique at a fixed RF frequency. In addition, PDMR detection of nuclear spins has been achieved in diamond.[36,37] Thus far, room-temperature detection of nuclear spins coupled to electron spins for defects in SiC has been achieved using pulsed electron-paramagnetic-resonance spectrometer,[41] an optical detection method via divacancies,[42] and a spin-dependent-recombination-based technique.[43] Although the third method involves the electrical detection of the nitrogen donor's nuclear spins in a bipolar junction transistor, this technique has not yet electrically detected either electron- or nuclear-spin coherence in SiC.

In the present work, we demonstrate PDMR of V2 centers using the frequency-sweep technique and electrical detection of ^{29}Si nuclear spins coupled to the V2 centers by combining PDMR and electron–nuclear double resonance (ENDOR).[44] The V2 centers operate at temperatures from cryogenic to room temperature, exhibiting excellent spin coherence;[45] they are also expected to be a promising resource for quantum information and quantum sensing.[17,46] The frequency-sweep technique enables a fast pulse sequence with multifrequency addressing, realizing the room-temperature electrical detection of nuclear spins coupled to V2 centers. Therefore, we expect these results to broaden the applicability of PDMR to quantum applications and to contribute to the realization of integrated quantum devices.

Figure 1(a) shows a schematic energy diagram for the V2 center in the bandgap.[20] The electron spin system is $S = 3/2$ in the ground state (GS)[47] and excited state (ES),[48] and the zero-phonon line is at 917 nm at low temperatures.[48] In addition, the V2 center has a long-lived metastable state (MS) with $S = 1/2$,[49] which provides a nonradiative and spin-dependent intersystem crossing (ISC), and the spin is initialized to $m_S = \pm 1/2$ by optical pumping.[50] PDMR occurs when a high-power laser is used to address the defect. Under high-power laser irradiation, the defect is excited from the GS to the ES and then

ionized from the ES by emitting one electron to the conduction band (CB). Because of the spin dependence of the ES lifetime, this photoionization probability is also spin-dependent, which results in spin-dependent photocurrent generation.[40] The ionization process changes the defect charge state to neutral, and it recovers to negative upon subsequent optical emission of a hole to the valence band (VB) with the photon energy above 0.9 eV.[20] This cycle of spin-dependent charge-state conversion is the basic mechanism of PDMR.

In the present study, we used a commercial 50-μm-thick n-type 4H-SiC epitaxial layer ([N] $= 7 \times 10^{14}$ cm^{-3}) on a 1-μm-thick n^+-type buffer layer ([N] $= 1 \times 10^{18}$ cm^{-3}) grown on an n-type substrate, purchased from Wolfspeed. We created the V2 centers by electron-beam irradiation at 2 MeV with a fluence of 1×10^{17} cm^{-2} and subsequent annealing under an Ar atmosphere at 600 °C for 30 min. PDMR currents were detected by a pair of electrodes fabricated on the sample via treatment with buffered hydrofluoric acid to remove the native oxide layer, followed by photolithography, metal deposition, and lift-off. The electrode was a Schottky type Ti contact (30 nm) covered with Pt 10 nm/Au 100 nm to prevent oxidation of the electrodes and enable wire-bonding. We constructed the custom-made PDMR measurement setup shown in Fig. 1(b). V2 centers were optically excited with a 905 nm laser pulsed with an acousto-optic modulator and focused with an air objective lens (NA = 0.75) fixed on a piezostage. The laser was focused on the cross point of the perpendicular electrode pair because the electrical field concentration and efficient photocurrent collection were expected. Given the transmittance of the objective lens, the typical laser power of the pulse was 72 mW. To manipulate both electron and nuclear spins, we used two high-frequency oscillators separately pulsed with microwave (MW) switches and subsequently amplified after mixing. In the present paper, we refer to the microwaves used for electron and nuclear spin manipulation as MW and RF, respectively. Afterward, MWs and RF were delivered to the V2
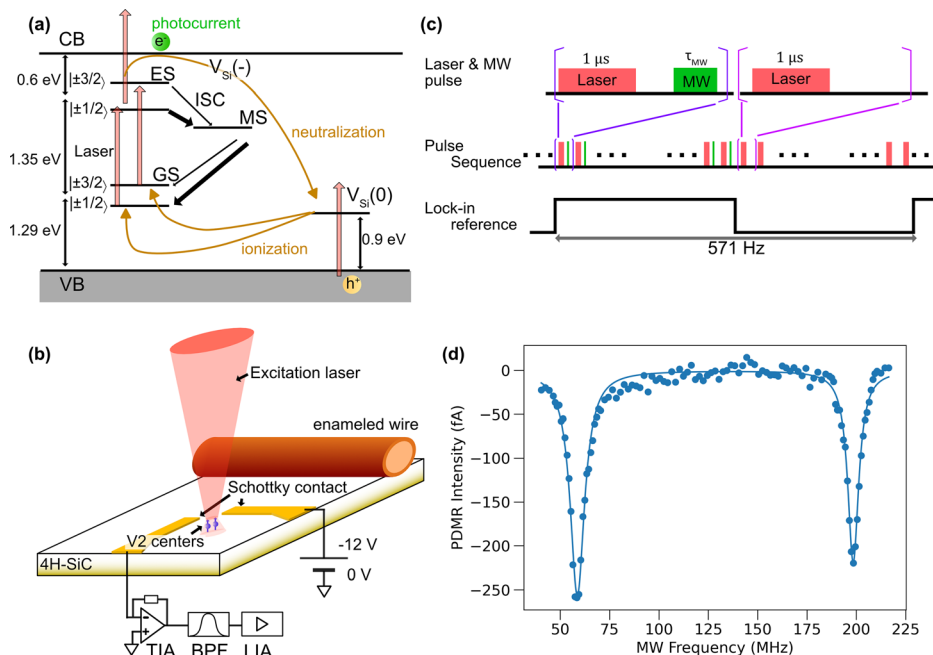

FIG. 1. (a) PDMR mechanism for V2 centers in 4H-SiC. Black arrows indicate ISC relaxation, and their thickness depicts the relaxation rate. Pink and yellow arrows indicate the laser excitation and charge state transition, respectively. (b) Schematic of the fabricated sample and measurement setup. (c) The pulse sequence for pPDMR measurement. Because of the bandwidth of the transimpedance amplifier, the entire pulse sequence was constructed by repeating a short sequence with the laser and MW pulse. For lock-in detection, the amplitude of the MWs was modulated at 571 Hz. (d) Observed pPDMR spectrum with $\tau_{MW} = 200$ ns (blue dots). The solid blue line is a Lorentzian fit.

centers via an enameled wire with a 50-μm-diameter copper core. We located the wire near the device ($\sim$50 μm from the detection position to the wire edge) to decrease the MW/RF power required to rotate the spins and thereby reduce MW/RF-induced noise. Also, insulating the wire from the devices may have contributed to noise reduction.

In the PDMR experiment, an external static magnetic field of approximately $\sim$4.56 mT was applied along the c-axis, parallel to the quantization axis of the V2 center. We used the device with an electrode pair with a gap of 6.9 μm, as estimated from optical microscopy observations, and applied a bias voltage of -12 V between the electrodes. The photocurrent was pre-amplified by a transimpedance amplifier (TIA, Femto Messtechnik DLPCA-200, gain $= 10^9$), passed through a 100 Hz-to-3 kHz bandpass filter (BPF, Stanford Research Systems SR560), and then detected by a lock-in amplifier (LIA, Stanford Research Systems SR830). Because the electrical detection bandwidth was limited to 1 kHz by the TIA, a single pulse sequence was repeated numerous times, and the MW was modulated at 571 Hz for lock-in detection.[35] The MW amplitude was modulated for the PDMR spectrum and Rabi oscillation experiments, and the phase was modulated for Ramsey, spin-echo, and ENDOR experiments. The modulation envelope and the lock-in reference signal were generated by a function generator (Tektronix AFG3021B).

We first present the results of frequency-sweep pulsed-PDMR (pPDMR) measurements with the pulse sequence shown in Fig. 1(c), with an MW pulse length $\tau_{MW} = 200$ ns at an input power of 24.5 dBm. The pPDMR spectrum resulting from the photocurrent change as a function of the MW frequency is shown in Fig. 1(d), without any background subtraction. The two peaks with a separation of 140.0 MHz $= 4D$ at frequencies of 58.4 and 198.4 MHz correspond to the transitions $|-1/2\rangle \leftrightarrow |-3/2\rangle$ and $|+1/2\rangle \leftrightarrow |+3/2\rangle$ of the V2 center, respectively, where $D = 35$ MHz (Ref. 48) is the GS zero-field splitting. Although the MW induces electric noise and the signal-to-noise ratio has been reported to worsen,[40] the coupling noise was suppressed in our system because we maintained a low MW power by locating the enameled wire in close proximity to the electrodes. Thus, our system enables observation of a clear PDMR spectrum by scanning the MW frequency, which is critical for fast and multifrequency quantum control in various applications, including an ENDOR experiment. We note that the negative signal is due to the negative bias voltage and that it becomes positive when the bias polarity is inverted. Photodetection at the identical position with an external photodiode and the same detection electronics gives positive contrast with a slight phase change irrespective of the bias polarity. Although determining the sign of the contrast with lock-in detection is not straightforward, we assign the PDMR spin contrast to be positive on resonances.

Next, we detected the electron spin coherence of the V2 centers using the PDMR technique. We first performed a Rabi experiment with the pulse sequence shown in Fig. 2(a). We drove the $|+1/2\rangle \leftrightarrow |+3/2\rangle$ transition by applying MWs at a frequency of 198.4 MHz with an input power of 23.7 dBm. The oscillating photocurrent was observed depending on the MW pulse length [Fig. 2(b)]. In addition to the oscillation, a background appeared and its intensity linearly increased with increasing pulse length. We attribute this background to the MW-induced noise. However, the background is low and additional background subtraction measurements like those used in the previous PDMR study[40] are unnecessary for the analysis. Direct fitting of the data with a damped cosine function plus a linear
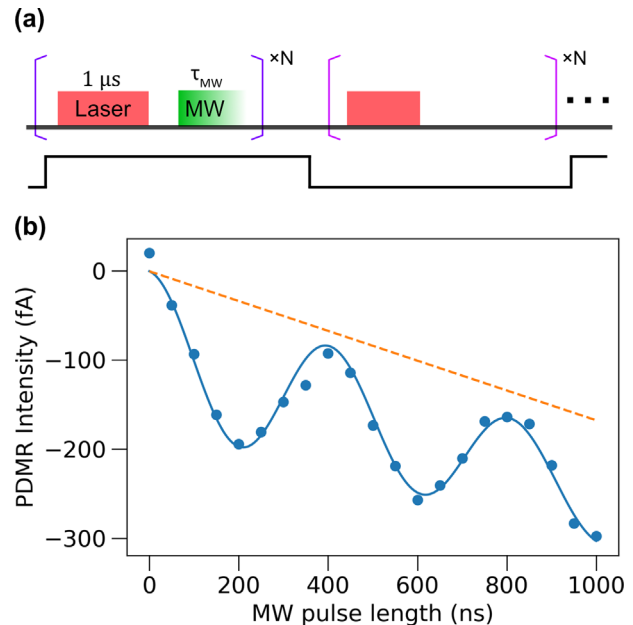

FIG. 2. Rabi experiment with PDMR: (a) the pulse sequence and (b) the experimental results (blue dots). The solid blue line is a fit with a damped cosine function plus a MW-pulse-length-dependent linear background (orange dashed line).

background gives a Rabi frequency of 4.93 ± 0.04 MHz. This result indicates that our PDMR technique enables coherent readout with a large signal-to-noise ratio even in the presence of MW coupling noise.

After determining the $\pi/2$ and π pulses to be 100 and 200 ns long, respectively, we measured the spin coherence by Ramsey interferometry and the spin-echo by PDMR. In the Ramsey interferometry measurement, we applied two MW $\pi/2$ pulses while varying the free-evolution time τ [Fig. 3(a)]. Here, the phase of the second pulse was modulated by $+x$ and $-x$ for lock-in detection, which projected the spin state to $m_s = 3/2$ and $1/2$, respectively. However, the photocurrent from other spin states and the MW-induced noise current were almost independent of the phase. Thus, subtracting the $-x$ pulse signal from the $+x$ pulse signal with lock-in detection can extract the spin signal while rejecting common-mode noise.[51] This phase-modulated-readout method was also used in the spin-echo and ENDOR experiments. For the precise estimation of T_2^*, an off-resonant measurement at the MW frequency of 168.4 MHz was separately performed to evaluate the common mode noise independent of τ. This nonzero but small baseline might originate from the noise at the modulation frequency from the function generator or from the MW phase modulation. As shown in Fig. 3(b), oscillating decay of the PDMR intensity depending on τ was observed. From the decay curve, we obtained $T_2^* = 311 \pm 18$ ns and an oscillation frequency of 4.57 ± 2.3 MHz. This oscillation frequency is very close to the detuning of the resonance frequency due to the hyperfine interaction with next-nearest-neighbor ^{29}Si nuclear spins.[52] The spin-echo was subsequently measured using a pulse sequence with three MW pulses of $(\pi/2)_{+x}$, $(\pi)_{+x}$, and alternate $(\pi/2)_{+x}$ (projection to $m_s = 1/2$) and $(\pi/2)_{-x}$ ($m_s = 3/2$) [Fig. 3(c)]. We obtained a stretched exponential decay curve against the free-evolution time τ [Fig. 3(d)]. As with the
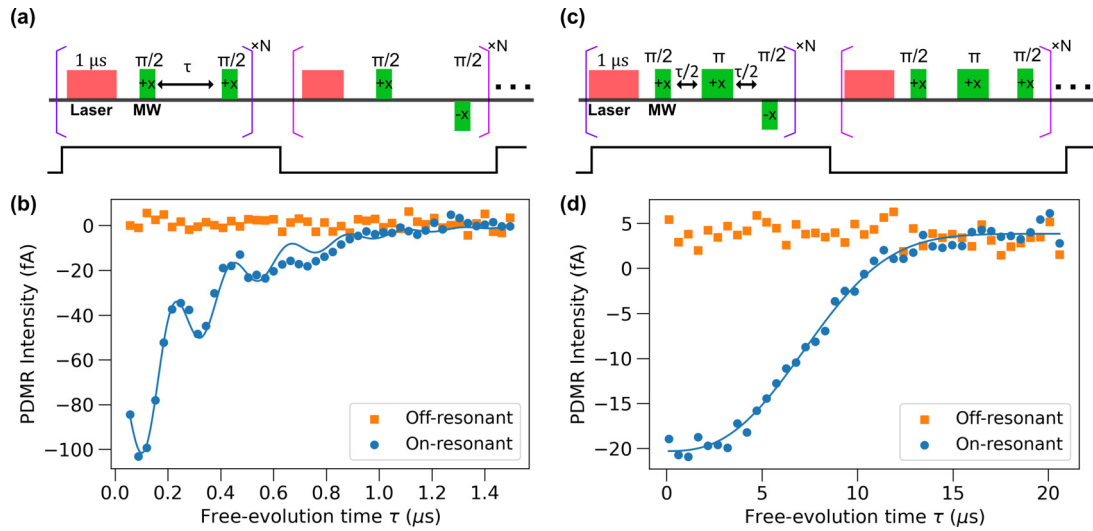
FIG. 3. Pulse sequence and results of the spin coherence control experiment with PDMR: (a) and (b) Ramsey interferometry measurement and (c) and (d) spin-echo measurement; $+x$ and $-x$ indicate the phase of the MWs in the pulse sequences. The off-resonant (orange squares) and on-resonant (blue dots) data are the experimental results obtained at MW frequencies of 168.4 and 198.4 MHz, respectively. Blue solid lines are fitting curves with an oscillating exponential decay and a stretched exponential decay for the Ramsey interferometry and spin-echo results, respectively.

Ramsey interferometry measurement, the off-resonant baseline was measured at 168.4 MHz, again independent of τ. We estimated the spin coherence time $T_2 = 8.6 \pm 0.1\ \mu s$, which agrees with the previous report for V2 centers under a comparable field strength and with a similar condition.[40] This series of results indicates that our PDMR technique can detect spin coherence, which is critical for quantum information and sensing applications. We subsequently used this echo detection for the nuclear spin detection by ENDOR.

Finally, we demonstrate the electrical detection of ^{29}Si nuclear spins in SiC by PDMR-based ENDOR (PD-ENDOR). We used the Davies ENDOR scheme;[53–55] its sequence is depicted in Fig. 4(a). We considered four levels: $|1/2 \uparrow\rangle$, $|1/2 \downarrow\rangle$, $|3/2 \uparrow\rangle$, and $|3/2 \downarrow\rangle$, where up and down arrows denote the ^{29}Si nuclear spin states of $m_I = +1/2$ and $-1/2$, respectively. After optical pumping of the electron spin into $m_s = 1/2$ with thermalized nuclear spin population, an MW π pulse that selectively flips $|1/2 \uparrow\rangle \leftrightarrow |3/2 \uparrow\rangle$ (transition A) was applied, followed by an RF pulse. When the RF pulse was resonant to a nuclear spin resonance transition between $|3/2 \uparrow\rangle \leftrightarrow |3/2 \downarrow\rangle$ (transition B), the spin population in the $|3/2 \uparrow\rangle$ decreased. Afterward, the selective spin-echo of transition A with the phase modulation allowed the PDMR readout of the population change only in the nuclear-spin $|\uparrow\rangle$ state. To find the resonance of the nuclear-spin-state selective transition for the PD-ENDOR experiment, we obtained a pPDMR spectrum clearly resolving the selective electron spin transitions [Fig. 4(b)]. A central peak at 197.7 MHz and two weak side peaks separated by 4.4 ± 0.1 MHz from the central peak were observed. These side peaks correspond to the nuclear-spin-selective transition between $|1/2 \downarrow\rangle \leftrightarrow |3/2 \downarrow\rangle$ and $|1/2 \uparrow\rangle \leftrightarrow |3/2 \uparrow\rangle$, respectively, which results from the hyperfine interaction with the NNN ^{29}Si. Although linewidth broadening was reported in a previous study involving nickel electrodes,[40] we observed a narrow linewidth of 2.02 ± 0.08 MHz, sufficient to resolve the hyperfine splitting; we attributed this narrow linewidth

to a smaller local magnetic field inhomogeneity resulting from the use of nonmagnetic electrodes. Figure 4(c) shows the Rabi oscillation with a low MW input power of 12.8 dBm at the central (197.7 MHz) and higher-frequency (202.1 MHz) transitions measured by PDMR. The analysis was performed in the manner previously described. We obtained Rabi frequencies of 1.29 ± 0.02 and 1.25 ± 0.02 MHz at MW frequencies of 197.7 and 202.1 MHz, respectively. For the PD-ENDOR experiment, we determined the MW pulses of π and $\pi/2$ to be 801 and 400 ns long, respectively, at the MW frequency of 202.1 MHz. Afterward, we performed PD-ENDOR using the pulse sequence shown in Fig. 4(d). Figure 4(e) shows the PD-ENDOR data acquired by scanning the frequency of a 3-μs-long RF pulse at an input power of 24.8 dBm. We observed three peaks at RF frequencies of 11.68 ± 0.02, 12.37 ± 0.03, and 12.81 ± 0.02 MHz. The peak intensity was $0.29 \pm 0.10 : 0.40 \pm 0.14 : 0.82 \pm 0.16$, or approximately 1:1:2. To determine the hyperfine constant for the obtained peaks, we consider the system Hamiltonian for the V2 center with an isotropic[41,56] hyperfine constant,

$$H = D\left(\hat{S}_z^2 - \frac{5}{4}\right) + \gamma_e B_z \hat{S}_z + A\left(\hat{S}_z \hat{I}_z + \hat{S}_x \hat{I}_x + \hat{S}_y \hat{I}_y\right) - \gamma_n B_z \hat{I}_z.$$

(1)

Here, $\hat{S}$ is the electron spin operator for $S = 3/2$, $\hat{I}$ is the nuclear spin operator for $I = 1/2$, $\gamma_e = 2.803 \times 10^4$ MHz/T and $\gamma_n = -8.465$ MHz/T is the gyromagnetic ratio for the electron spin and the ^{29}Si nuclear spin, respectively, $B_z = 4.56$ mT is an external magnetic field aligned along the z-axis, and $A > 0$ is the isotropic hyperfine constant for the NNN ^{29}Si. By diagonalizing H, the eigenvalues ν in a frequency unit for $|+3/2 \uparrow\rangle$ and $|+3/2 \downarrow\rangle$ are given by

$$\nu\left(+\frac{3}{2}\uparrow\right) = D + \frac{3}{2}\gamma_e B_z - \frac{1}{2}\gamma_n B_z + \frac{3}{4}A,$$
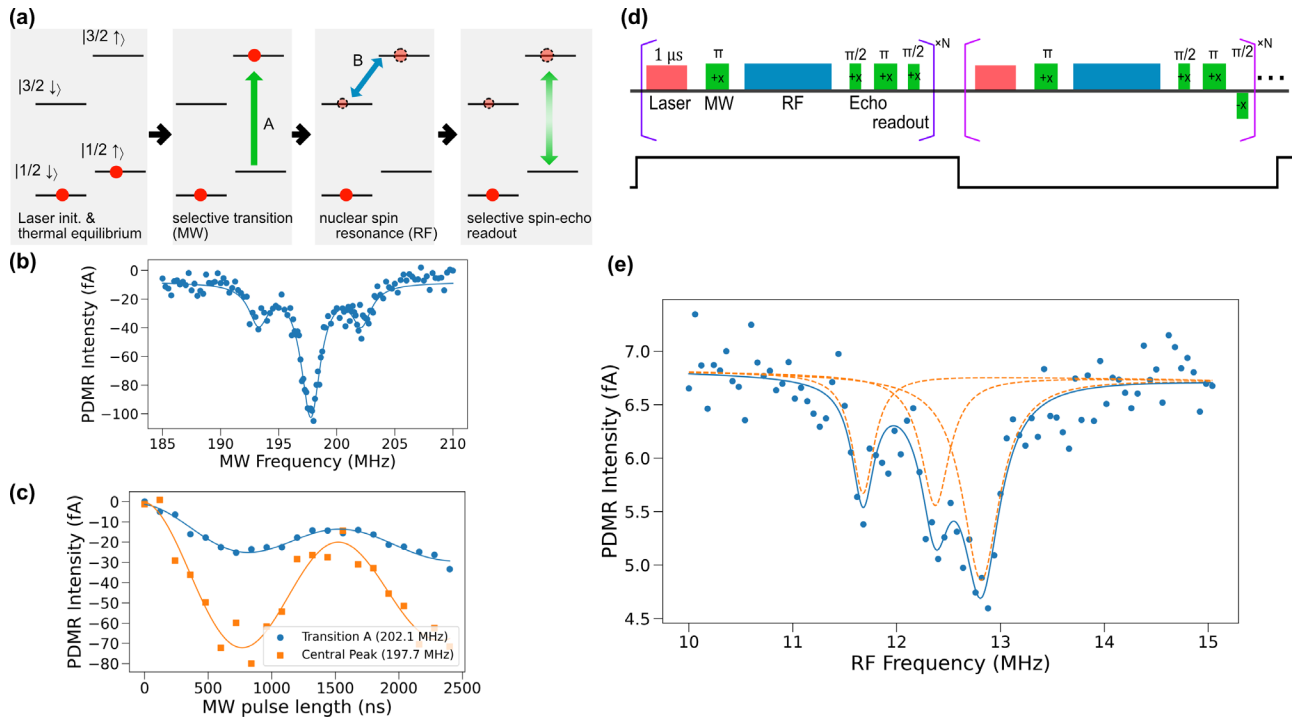
(2)

FIG. 4. (a) Schematic of the ENDOR sequence for V2 centers coupled with ^{29}Si nuclear spins of $I = 1/2$, where ↑ and ↓ indicate the nuclear spin state of $m_I = +1/2$ and $-1/2$, respectively. (b) pPDMR spectrum showing the hyperfine structure of the V2 centers for the electron spin transition $|+1/2\rangle \leftrightarrow |+3/2\rangle$ (blue dots). The solid blue line is a fit line. (c) Rabi oscillation of the transition $|+1/2\rangle \leftrightarrow |+3/2\rangle$ at MW frequencies of 202.1 MHz (high-frequency side peak, blue dots) and 197.7 MHz (central peak, orange squares), respectively. Blue and orange solid lines are fits using a damped cosine function plus a linear background for each result. (d) Pulse sequence of PD-ENDOR measurement based on the Davies ENDOR scheme, where $+x$ and $-x$ indicate the phase of the MW pulse. (e) PD-ENDOR spectrum corresponding to the nuclear magnetic resonance transition $|+3/2 \uparrow\rangle \leftrightarrow |+3/2 \downarrow\rangle$ (blue dots). The blue solid and orange dashed lines are fits for the whole spectrum and individual peaks, respectively.

$$\nu\left(+\frac{3}{2}\downarrow\right) = \gamma_e B_z - \frac{1}{4}A + \sqrt{\left\{D + \frac{1}{2}(\gamma_e + \gamma_n)B_z - \frac{1}{2}A\right\}^2 + \frac{3}{4}A^2}.$$

$$(3)$$

The analytical calculation of the nuclear spin resonance from Eqs. (2) and (3) results in

$$A = \frac{(2D + \gamma_e B_z - f)(\gamma_n B_z + f)}{3D + \frac{3}{2}\gamma_e B_z - \frac{1}{2}\gamma_n B_z - 2f},$$

$$(4)$$

where $f = \nu(+3/2 \uparrow) - \nu(+3/2 \downarrow)$ is the ENDOR peak frequency in $|+3/2\rangle$. Note that this equation is derived without a high-field approximation to consider the weak magnetic field. From the analysis, the peaks at 11.68, 12.37, and 12.81 MHz correspond to isotropic hyperfine constants of 7.92 ± 0.02, 8.41 ± 0.02, and 8.72 ± 0.02 MHz, respectively. A first-principles study[39] suggests that there are three nonequivalent sites for NNN ^{29}Si with a multiplicity of 1:1:2, which agrees with our observation. However, in an experimental ENDOR study with a W-band spectrometer at 100 K,[50] the hyperfine constant for the NNN ^{29}Si for V2 centers was reported to have four values—7.90, 8.62, 8.74, and 8.81 MHz—which the authors attributed to the slightly nonequivalent sites for NNN Si. The hyperfine constants obtained by our PD-ENDOR experiment agree well with those from the W-band study, except for $A = 8.41$ MHz. Although peak

assignment remains an additional task, this result indicates that our PDMR technique can resolve several ENDOR peaks with different hyperfine constants and might enable selective coherent control of nuclear spins, facilitating the development of electrical-driven integrated quantum applications.

In summary, suppressing the MW coupling noise by using a wire antenna located near the electrodes, we achieved the electrical detection of V2 centers in 4H-SiC using frequency-scanning PDMR under a static magnetic field, and demonstrated electrical observation of coherence control and hyperfine interaction. We expect that further optimization of the MW antenna using direct microfabrication on the chip will improve the signal-to-noise ratio. In addition, we showed PD-ENDOR of ^{29}Si nuclear spins coupled to the V2 centers under ambient conditions. The results indicate that the PDMR and PD-ENDOR techniques can potentially access nuclear spins in SiC as quantum memory and enable the development and integration of quantum devices that operate under ambient conditions. Therefore, this work represents a critical advancement toward scalable quantum applications using SiC.

AUTHOR DECLARATIONS
Conflict of Interest

The authors have no conflicts to disclose.

Author Contributions

Tetsuri Nishikawa: Data curation (equal); Formal analysis (lead); Investigation (equal); Methodology (equal); Software (supporting); Validation (equal); Visualization (lead); Writing – original draft (equal); Writing – review & editing (equal). **Naoya Morioka:** Conceptualization (equal); Data curation (equal); Formal analysis (supporting); Funding acquisition (supporting); Investigation (equal); Methodology (equal); Project administration (supporting); Resources (supporting); Software (lead); Supervision (supporting); Validation (equal); Visualization (supporting); Writing – original draft (equal); Writing – review & editing (equal). **Hiroshi Abe:** Resources (equal); Writing – review & editing (supporting). **Hiroki Morishita:** Methodology (supporting); Resources (supporting); Writing – review & editing (supporting). **Takeshi Ohshima:** Funding acquisition (supporting); Resources (equal); Writing – review & editing (supporting). **Norikazu Mizuochi:** Conceptualization (equal); Funding acquisition (lead); Methodology (equal); Project administration (lead); Resources (equal); Supervision (lead); Writing – original draft (supporting); Writing – review & editing (equal).

DATA AVAILABILITY

The data that support the findings of this study are available from the corresponding authors upon reasonable request.

REFERENCES

[1]C. L. Degen, F. Reinhard, and P. Cappellaro, Rev. Mod. Phys. **89**, 035002 (2017).

[2]Y. Wu, F. Jelezko, M. B. Plenio, and T. Weil, Angew. Chem., Int. Ed. **55**, 6586 (2016).

[3]M. E. Bathen and L. Vines, Adv. Quantum Technol. **4**, 2100003 (2021).

[4]N. T. Son, C. P. Anderson, A. Bourassa, K. C. Miao, C. Babin, M. Widmann, M. Niethammer, J. Ul Hassan, N. Morioka, I. G. Ivanov, F. Kaiser, J. Wrachtrup, and D. D. Awschalom, Appl. Phys. Lett. **116**, 190501 (2020).

[5]S. Castelletto and A. Boretti, J. Phys. Photonics **2**, 022001 (2020).

[6]T. Wolf, P. Neumann, K. Nakamura, H. Sumiya, T. Ohshima, J. Isoya, and J. Wrachtrup, Phys. Rev. X **5**, 041001 (2015).

[7]G. Balasubramanian, I. Y. Chan, R. Kolesov, M. Al-Hmoud, J. Tisler, C. Shin, C. Kim, A. Wojcik, P. R. Hemmer, A. Krueger, T. Hanke, A. Leitenstorfer, R. Bratschitsch, F. Jelezko, and J. Wrachtrup, Nature **455**, 648 (2008).

[8]P. Neumann, I. Jakobi, F. Dolde, C. Burk, R. Reuter, G. Waldherr, J. Honert, T. Wolf, A. Brunner, J. H. Shim, D. Suter, H. Sumiya, J. Isoya, and J. Wrachtrup, Nano Lett. **13**, 2738 (2013).

[9]E. D. Herbschleb, H. Kato, Y. Maruyama, T. Danjo, T. Makino, S. Yamasaki, I. Ohki, K. Hayashi, H. Morishita, M. Fujiwara, and N. Mizuochi, Nat. Commun. **10**, 3766 (2019).

[10]F. Jelezko, T. Gaebel, I. Popa, M. Domhan, A. Gruber, and J. Wrachtrup, Phys. Rev. Lett. **93**, 130501 (2004).

[11]Y. Sekiguchi, Y. Yasui, K. Tsurumoto, Y. Koga, R. Reyes, and H. Kosaka, Commun. Phys. **4**, 264 (2021).

[12]T. Xie, Z. Zhao, X. Kong, W. Ma, M. Wang, X. Ye, P. Yu, Z. Yang, S. Xu, P. Wang, Y. Wang, F. Shi, and J. Du, Sci. Adv. **7**, eabg9204 (2021).

[13]N. Kalb, A. A. Reiserer, P. C. Humphreys, J. J. W. Bakermans, S. J. Kamerling, N. H. Nickerson, S. C. Benjamin, D. J. Twitchen, M. Markham, and R. Hanson, Science **356**, 928 (2017).

[14]W. F. Koehl, B. B. Buckley, F. J. Heremans, G. Calusine, and D. D. Awschalom, Nature **479**, 84 (2011).

[15]C. P. Anderson, A. Bourassa, K. C. Miao, G. Wolfowicz, P. J. Mintun, A. L. Crook, H. Abe, J. Ul Hassan, N. T. Son, T. Ohshima, and D. D. Awschalom, Science **366**, 1225 (2019).

[16]A. Bourassa, C. P. Anderson, K. C. Miao, M. Onizhuk, H. Ma, A. L. Crook, H. Abe, J. Ul-Hassan, T. Ohshima, N. T. Son, G. Galli, and D. D. Awschalom, Nat. Mater. **19**, 1319 (2020).

[17]M. Niethammer, M. Widmann, S.-Y. Lee, P. Stenberg, O. Kordina, T. Ohshima, N. T. Son, E. Janzén, and J. Wrachtrup, Phys. Rev. Appl. **6**, 034001 (2016).

[18]A. N. Anisimov, D. Simin, V. A. Soltamov, S. P. Lebedev, P. G. Baranov, G. V. Astakhov, and V. Dyakonov, Sci. Rep. **6**, 33301 (2016).

[19]N. Morioka, C. Babin, R. Nagy, I. Gediz, E. Hesselmeier, D. Liu, M. Joliffe, M. Niethammer, D. Dasari, V. Vorobyov, R. Kolesov, R. Stöhr, J. Ul-Hassan, N. T. Son, T. Ohshima, P. Udvarhelyi, G. Thiering, A. Gali, J. Wrachtrup, and F. Kaiser, Nat. Commun. **11**, 2516 (2020).

[20]M. Widmann, M. Niethammer, D. Y. Fedyanin, I. A. Khramtsov, T. Rendler, I. D. Booker, J. Ul Hassan, N. Morioka, Y.-C. Chen, I. G. Ivanov, N. T. Son, T. Ohshima, M. Bockstedte, A. Gali, C. Bonato, S.-Y. Lee, and J. Wrachtrup, Nano Lett. **19**, 7173 (2019).

[21]M. Widmann, S.-Y. Lee, T. Rendler, N. T. Son, H. Fedder, S. Paik, L.-P. Yang, N. Zhao, S. Yang, I. Booker, A. Denisenko, M. Jamali, S. A. Momenzadeh, I. Gerhardt, T. Ohshima, A. Gali, E. Janzén, and J. Wrachtrup, Nat. Mater. **14**, 164 (2015).

[22]H. Jurgen von Bardeleben, J.-L. Cantin, U. Gerstmann, W. G. Schmidt, and T. Biktagirov, Nano Lett. **21**, 8119 (2021).

[23]S. A. Zargaleh, B. Eble, S. Hameau, J.-L. Cantin, L. Legrand, M. Bernard, F. Margaillan, J.-S. Lauret, J.-F. Roch, H. J. von Bardeleben, E. Rauls, U. Gerstmann, and F. Treussart, Phys. Rev. B **94**, 060102 (2016).

[24]J.-F. Wang, F.-F. Yan, Q. Li, Z.-H. Liu, H. Liu, G.-P. Guo, L.-P. Guo, X. Zhou, J.-M. Cui, J. Wang, Z.-Q. Zhou, X.-Y. Xu, J.-S. Xu, C.-F. Li, and G.-C. Guo, Phys. Rev. Lett. **124**, 223601 (2020).

[25]G. Yusa, K. Muraki, K. Takashina, K. Hashimoto, and Y. Hirayama, Nature **434**, 1001 (2005).

[26]G. D. Fuchs, G. Burkard, P. V. Klimov, and D. D. Awschalom, Nat. Phys. **7**, 789 (2011).

[27]P. C. Maurer, G. Kucsko, C. Latta, L. Jiang, N. Y. Yao, S. D. Bennett, F. Pastawski, D. Hunger, N. Chisholm, M. Markham, D. J. Twitchen, J. I. Cirac, and M. D. Lukin, Science **336**, 1283 (2012).

[28]S. Zaiser, T. Rendler, I. Jakobi, T. Wolf, S.-Y. Lee, S. Wagner, V. Bergholm, T. Schulte-Herbrüggen, P. Neumann, and J. Wrachtrup, Nat. Commun. **7**, 12279 (2016).

[29]Y. Matsuzaki, T. Shimo-Oka, H. Tanaka, Y. Tokura, K. Semba, and N. Mizuochi, Phys. Rev. A **94**, 052330 (2016).

[30]M. Pfender, N. Aslam, H. Sumiya, S. Onoda, P. Neumann, J. Isoya, C. A. Meriles, and J. Wrachtrup, Nat. Commun. **8**, 834 (2017).

[31]N. Mizuochi, P. Neumann, F. Rempp, J. Beck, V. Jacques, P. Siyushev, K. Nakamura, D. J. Twitchen, H. Watanabe, S. Yamasaki, F. Jelezko, and J. Wrachtrup, Phys. Rev. B **80**, 041201 (2009).

[32]B. Smeltzer, J. McIntyre, and L. Childress, Phys. Rev. A **80**, 050302 (2009).

[33]E. Bourgeois, A. Jarmola, P. Siyushev, M. Gulka, J. Hruby, F. Jelezko, D. Budker, and M. Nesladek, Nat. Commun. **6**, 8577 (2015).

[34]F. M. Hrubesch, G. Braunbeck, M. Stutzmann, F. Reinhard, and M. S. Brandt, Phys. Rev. Lett. **118**, 037601 (2017).

[35]M. Gulka, E. Bourgeois, J. Hruby, P. Siyushev, G. Wachter, F. Aumayr, P. R. Hemmer, A. Gali, F. Jelezko, M. Trupke, and M. Nesladek, Phys. Rev. Appl. **7**, 044032 (2017).

[36]H. Morishita, S. Kobayashi, M. Fujiwara, H. Kato, T. Makino, S. Yamasaki, and N. Mizuochi, Sci. Rep. **10**, 792 (2020).

[37]M. Gulka, D. Wirtitsch, V. Ivády, J. Vodnik, J. Hruby, G. Magchiels, E. Bourgeois, A. Gali, M. Trupke, and M. Nesladek, Nat. Commun. **12**, 4421 (2021).

[38]T. Murooka, M. Shiigai, Y. Hironaka, T. Tsuji, B. Yang, T. M. Hoang, K. Suda, K. Mizuno, H. Kato, T. Makino, M. Ogura, S. Yamasaki, M. Hatano, and T. Iwasaki, Appl. Phys. Lett. **118**, 253502 (2021).

[39]V. Ivády, J. Davidsson, N. T. Son, T. Ohshima, I. A. Abrikosov, and A. Gali, Phys. Rev. B **96**, 161114 (2017).

[40]M. Niethammer, M. Widmann, T. Rendler, N. Morioka, Y.-C. Chen, R. Stöhr, J. U. Hassan, S. Onoda, T. Ohshima, S.-Y. Lee, A. Mukherjee, J. Isoya, N. T. Son, and J. Wrachtrup, Nat. Commun. **10**, 5569 (2019).

[41]N. Mizuochi, S. Yamasaki, H. Takizawa, N. Morishita, T. Ohshima, H. Itoh, T. Umeda, and J. Isoya, Phys. Rev. B **72**, 235208 (2005).

[42]P. V. Klimov, A. L. Falk, D. J. Christle, V. V. Dobrovitski, and D. D. Awschalom, Sci. Adv. **1**, e1501015 (2015).

[43]R. J. Waskiewicz, B. R. Manning, D. J. McCrory, and P. M. Lenahan, J. Appl. Phys. **126**, 125709 (2019).

[44]G. Feher, Phys. Rev. **103**, 834 (1956).

[45]D. Simin, H. Kraus, A. Sperlich, T. Ohshima, G. V. Astakhov, and V. Dyakonov, Phys. Rev. B **95**, 161201 (2017).

[46]J. B. S. Abraham, C. Gutgsell, D. Todorovski, S. Sperling, J. E. Epstein, B. S. Tien-Street, T. M. Sweeney, J. J. Wathen, E. A. Pogue, P. G. Brereton, T. M. McQueen, W. Frey, B. D. Clader, and R. Osiander, Phys. Rev. Appl. **15**, 064022 (2021).

[47]N. Mizuochi, S. Yamasaki, H. Takizawa, N. Morishita, T. Ohshima, H. Itoh, and J. Isoya, Phys. Rev. B **66**, 235202 (2002).

[48]E. Janzén, A. Gali, P. Carlsson, A. Gällström, B. Magnusson, and N. T. Son, Physica B **404**, 4354 (2009).

[49]Ö. O. Soykal, P. Dev, and S. E. Economou, Phys. Rev. B **93**, 081207 (2016).

[50]V. A. Soltamov, B. V. Yavkin, G. V. Mamin, S. B. Orlinskii, I. D. Breev, A. P. Bundakova, R. A. Babunts, A. N. Anisimov, and P. G. Baranov, Phys. Rev. B **104**, 125205 (2021).

[51]N. Bar-Gill, L. M. Pham, A. Jarmola, D. Budker, and R. L. Walsworth, Nat. Commun. **4**, 1743 (2013).

[52]M. Wagner, N. Q. Thinh, N. T. Son, W. M. Chen, E. Janzén, P. G. Baranov, E. N. Mokhov, C. Hallin, and J. L. Lindström, Phys. Rev. B **66**, 155214 (2002).

[53]E. R. Davies, Phys. Lett. A **47**, 1 (1974).

[54]F. Hoehne, L. Dreher, H. Huebl, M. Stutzmann, and M. S. Brandt, Phys. Rev. Lett. **106**, 187601 (2011).

[55]A. Schweiger and G. Jeschke, *Principles of Pulse Electron Paramagnetic Resonance* (Oxford University Press, 2001).

[56]T. Wimbauer, B. K. Meyer, A. Hofstaetter, A. Scharmann, and H. Overhof, Phys. Rev. B **56**, 7384 (1997).